# Structural investigation on the (1-*x*)Pb($Mg_{1/3}Nb_{2/3}$)$O_3$-*x*$PbTiO_3$ (*x*=0; 0.21) solid solution using powder diffraction

H. Wang[1,*], H. Ehrenberg[1,2], A. Senyshyn[1,3], R. Schierholz[1], J.-C. Jaud[1], H. Fuess[1]

[1] Institute for Materials Science, Darmstadt University of Technology, Petersenstr. 23, D-64287 Darmstadt, Germany
[2] Institute for Complex Materials, IFW Dresden, Helmholtzstr.20, D-01069 Dresden, Germany
[3] Forschungsneutronenquelle Heinz Maier-Leibnitz (FRM II), Technische Universität München, Lichtenbergstr. 1, D-85747 Garching b. München, Germany
[*] saliencas@hotmail.com

**Keywords**: powder diffraction, Rietveld method, electron diffraction, PMN-PT

**Abstract.** A structural investigation of the complex perovskite ferroelectrics (1-*x*)Pb($Mg_{1/3}Nb_{2/3}$)$O_3$-*x*$PbTiO_3$ (= PMN-PT) was carried out by X-ray and neutron powder diffraction. Qualitative phase analysis using Rietveld method combined with electron diffraction was performed for compositions in the PMN-rich region. A ferroelectric state of a rhombohedral symmetry (*R3mH*) gradually developed with the input of titanate to cubic PMN (*Pm3m*), as further evidenced by hysteresis loops measured and domain contrast observed in dark field imaging. Intrinsic local structure due to atomic mismatch seems to be the main reason for the complexity of this disordered system.

## Introduction

Ferroelectric materials exhibit high dielectric permittivity and piezoelectricity and are widely used as transducers and electronic components. Compounds actually used are complex mixed-ion perovskite, such as relaxor ferroelectrics PMN-PT, that exhibit superior piezoelectric and electromechanical properties over a wide range of composition compared with commercial $PbZr_{1-x}Ti_xO_3$ [1,2]. PMN prototype relaxors showed the existence of two components—an isotropic spherical glass matrix and anisotropic ferroelectric (FE) nanoclusters [3,4]. Also, Pb nuclei are displaced in the spherical glass matrix at 290 K ($T_C$=210 K), but there is no preferential frozen orientation or magnitude of displacement. Neutron diffraction revealed a drastic increase of the volume and correlation lengths of polar nanoregions (PNRs) below 200 K [5]. Two different atomic displacements $\delta_{c.m}$ (caused by

soft-mode condensation) and $\delta_{shift}$ (a uniform displacement of PNRs along their polar direction) were proposed below the Burns temperature of a PMN crystal by neutron diffuse scattering [6]. Neutron diffraction of PMN crystals reveals a strong lattice distortion and depth dependence in the surface region over a length scale of 100μm [7]. These phenomena indicate that PMN is an incipient FE, also found in PMN-PT crystals for $0<x<0.21$ from dielectric and domain studies [8,9]. This "hidden" transition nature (seen in unpoled samples but not as clearly as in the poled samples) was enhanced by an *E* field [8] associated with the appearance of polar microdomains. Since the nanodomain size is much smaller than the coherence length of diffraction radiation, scattered waves from individual nanodomains coherently superimpose during diffraction, thus, significant broadening of the reflection is expected. Consequently, the observed *tetragonal*-phase nanotwins with a domain size about 10 nm by transmission electron microscopy in PMN-PT ($x$=0.33) [10] appear to be the monoclinic $M_C$ phase in low-resolution diffraction & polarized light microscopy.
Recent neutron and X-ray scattering studies on PMN-PT crystals ($x$<0.25) in zero E-field found no long-range structural distortion in the bulk at very low temperatures, therefore this new phase is referred as unkown phase-*X* [11,12]. High-energy XRD results of PZN-PT crystals also show that skin effects in distinct outer layers (10–50μm) are present in all samples [13]. Recently a *R* phase was found to develop in both the outer layer and crystal interior with increasing Ti content, seen in a PMN-PT ($x$=0.27) crystal [12]. The polarization of FE nanoclusters and boundary conditions near the surface are believed to play an essential role in the surface distortion. Addition of Ti tends to decrease chemical ordered domain size and increase the ferroelectrically active polar domains in the PMN-PT system. Powder neutron diffraction studies [14] of PMN-PT ($0.25\leq x\leq 0.39$) with compositions across the morphotropic phase boundary construct a phase diagram showing stability regions of monoclinic $M_B$, monoclinic $M_C$, tetragonal and cubic phases. Due to the existence of unkown *X* phase in the PMN-rich side, the interactions between the cationic ordered chemical domains and the growing polar domains would be highly interesting. As presented above, great attention was paid to microstructures related to special properties, but the true symmetry is still under controversy [11-14]. To clarify the relevance of structural aspects in physical mechanisms for such complex systems, which is critical for their applications, we aim to clarify the basic structure using neutron powder diffraction.

# Experimental procedure

Well-grown PMN-PT ($x$=0, 0.21) crystals [15] were treated by grinding into fine powder in an agate mortar and annealed at about 900 K. The structure of powder samples was first recorded to be a pure phase in glass capillaries with well-match amount by X-ray measurement with transmission geometry (Mo wavelength 0.7093Å). The overall measuring time for one sample was 12 hours to have very good counting statistics over the angular range 3-50° (in 2theta) while rotating the samples during data collection. Constant wavelength neutron powder diffraction (NPD) experiments were carried out on the neutron powder diffractometer SPODI at FRM II, Garching, Germany [16]. The wavelength of 1.5482 Å was obtained at 155° take off angle from a (551) reflection of composite Ge monochromator. Two dimensional powder diffraction patterns were collected using a multidetector consisting of 80 $^3$He vertical position-sensitive (300 mm effective height) tubes. The powdered sample was contained into a thin wall (0.15 mm thickness) vanadium can,

which was further mounted into a top-loading closed cycle refrigerator and cooled down to 3 K. Data sets were recorded at 300K and 3K in a 2theta range of 0–155° with Δ2θ steps of 0.04°. The full profile Rietveld method implemented in the FullProf suite of programs was applied to analyze powder patterns [17]. The peak profile shape was described by a modified Thompson-Cox-Hastings pseudo-Voigt function. The background of the diffraction pattern was fitted using a linear interpolation between selected data points in non-overlapping regions. The scale factor, lattice parameters, fractional coordinates of atomic sites and their isotropic displacement parameters, zero angular shift, profile shape parameters and half width (Caglioti) parameters were refined. For PMN it was found that the refinement of anisotropic thermal displacement parameters for Nb/Mg sites improved significantly the fitting, whereas the displacements of Pb and O for PMN-PT (0.21) were described by 2nd rank tensors.

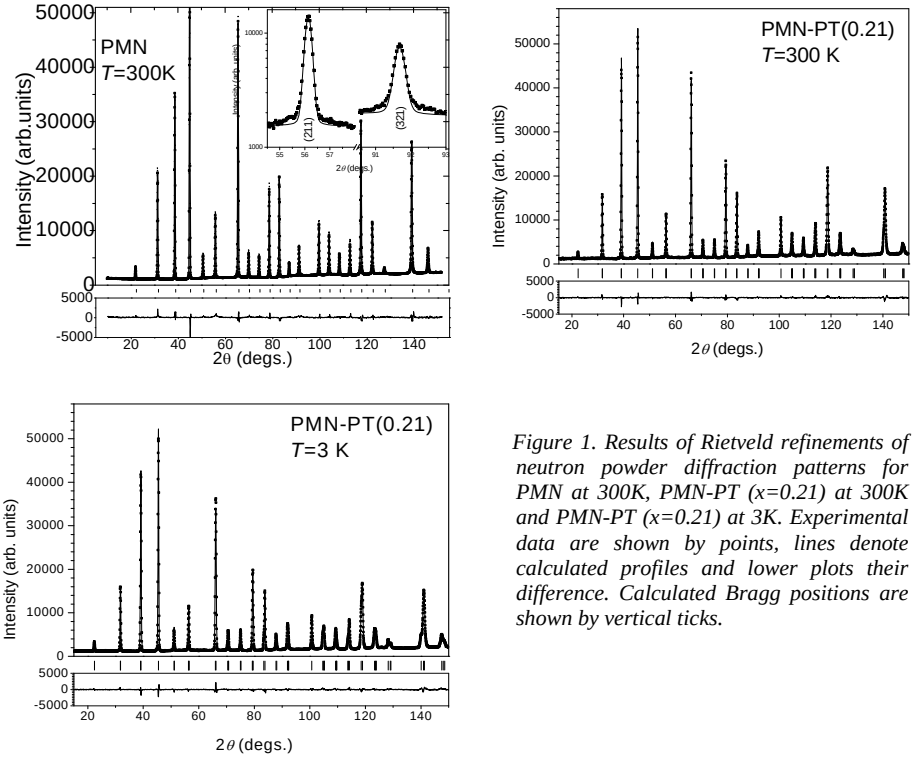


*Figure 1. Results of Rietveld refinements of neutron powder diffraction patterns for PMN at 300K, PMN-PT (x=0.21) at 300K and PMN-PT (x=0.21) at 3K. Experimental data are shown by points, lines denote calculated profiles and lower plots their difference. Calculated Bragg positions are shown by vertical ticks.*

Crystal samples for transmission electron microscopy were prepared by the procedure of sawing, polishing, dimpling, and ion milling [18]. Transmission electron microscopy was performed with a Philips CM20 operating at 200 kV for imaging and selected area electron diffraction (SAED) and at 80 kV for convergent-beam electron diffraction (CBED) with a double-tilt holder. The hysteresis (P-E) loops were obtained using a Sawyer-Tower circuit at 1 Hz and at different temperatures.

# Results and discussion

The well fitted neutron diffraction patterns of pure PMN and PMN-PT ($x$=0.21) are shown in figure 1. The final refined atomic coordinates and isotropic displacement parameters (except Pb and O for $x$=0.21) for the two samples are reported in table 1. In these two samples, mixed cation site occupancies of $Mg^{2+}/Nb^{5+}/Ti^{4+}$ were calculated from their nominal compositions. For the structural study of pure PMN, we assumed a cubic symmetry with space group *Pm-3m*. In the early stages of PMN refinements, constraints on the cubic model were introduced initially with ideal sites. The ambient cubic structure of PMN seems even more complicated than the normal perovskite one due to the appearence of diffuse scattering shown in figure 1 (inset), seen also e.g. reference [7,19], where the decrease of intensity of diffuse scattering with the addition of Ti was observed. It seems to be the reason why the ideal cubic model slightly mismatched without involving the local structure characteristics.

*Table 1. Final refined coordinates and displacement parameters (Å$^2$).*

| Compound | | PMN | PMN-PT (0.21) | |
|---|---|---|---|---|
| Temperature, K | | 300 | 300 | 3 |
| Space group | | *Pm-3m* | *R3mH* | *R3mH* |
| Lattice parameters, Å | | a=4.04551(1) | a=5.69497(3)<br>c=6.99061(5) | a=5.68961(3)<br>c=6.99761(5) |
| *Pb*, | *x/a* | 0 | 0 | 0 |
| | *y/b* | 0.0562(8) | 0 | 0 |
| | *z/c* | 0.0562(8) | 0.5539(4) | 0.5526(2) |
| $u_{iso}$, Å$^2$ | | 0.0082(15) | 0.0279(4) | 0.0279(4) |
| $u_{11}$, $u_{22}$, | | | 0.0326(5), | |
| $u_{33}$, $u_{12}$, | | | 0.0326(5), | 0.0291(4), 0.0291(4), |
| $u_{13}$, $u_{23}$ | | — | 0.0013(2), | 0.0048(3), 0.0146(2), |
| | | | 0.0163(2), | 0, 0 |
| | | | 0, 0 | |
| Nb/Mg(/Ti), | *x/a* | ½ | 0 | 0 |
| | *y/b* | ½ | 0 | 0 |
| | *z/c* | ½ | 0.02475 | 0.02475 |
| $u_{iso}$, Å$^2$ | | 0.00306(17) | 0.02(2) | 0.0002(2) |
| $u_{11}$, $u_{22}$, | | 0.00306(17), 0.00306(17), | | |
| $u_{33}$, $u_{12}$, | | 0.00306(17), 0, | — | — |
| $u_{13}$, $u_{23}$ | | 0, 0 | | |
| O, | *x/a* | 0.0021(1) | 0.3366(3) | 0.3388(2) |
| | *y/b* | 0.540(3) | 0.1678(1) | 0.16891(8) |
| | *z/c* | 0.520(5) | 0.1894(7) | 0.1690(3) |
| $u_{iso}$, Å$^2$ | | 0.0040(3) | 0.0193(4) | 0.0090(3) |
| $u_{11}$, $u_{22}$, | | | 0.0060(5), | |
| $u_{33}$, $u_{12}$, | | | 0.0120(3), | 0.0056(3), 0.0056(3), |
| $u_{13}$, $u_{23}$ | | — | 0.0134(5), | 0.0034(2), 0.0028(2), |
| | | | 0.0030(2), | -0.0023(2), |
| | | | -0.0044(3), | -0.00115(8) |
| | | | -0.0022(1) | |
| $R_p$, $R_{wp}$ | | 4.39, 5.86 | 3.03, 3.82 | 3.39, 4.32 |
| $R_{exp}$, $\chi^2$ | | 2.17, 7.31 | 2.18, 3.08 | 2.23, 3.77 |

For PMN-PT ($x$=0.21) the effort to refine its crystal structure in a cubic model failed, whereas fairly promising results were obtained using a rhombohedral one. Therefore, at 3

and 300 K, we used space group setting *R3mH*. In the asymmetric unit of the structure of the rhombohedral phase during the Rietveld refinement, $Pb^{2+}$ and $Nb^{5+}/Ti^{4+}/Mg^{2+}$ ions occupy 3(*a*) sites at (0,0,*z*) and $O^{2-}$ at the 9(*b*) site at (2*x*,*x*,*z*).

To understand the effects visible in the diffraction pattern of samples with different compositions, we performed transmission electron microscopy and electron diffraction. As seen in figure 2, domain contrast was found in dark field image close to [01-1] incidence with intersecting domains in [100] and [011] and inner contrast within the domains. The SAED shows superlattice reflections of type ½½½, probably due to chemical ordering [20]. The First Order Laue-Zone in the [1-11] CBED Pattern shows a deviation from cubic symmetry, by revealing only symmetry m instead of 3m.

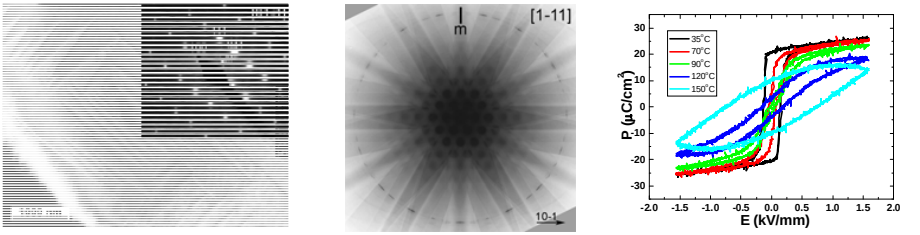


*Figure 2. Left: Dark field image and corresponding SAED [01-1]c zone axis for PMN-PT crystal x=0.21. Middle: <111> incidence CBED-pattern recorded at 80 kV on a crushed sample revealing only mirror symmetry. Right: Hysteresis loops of PMN-PT (x=0.21) crystal.*

Recently, the transformation of spontaneous ferroelectric to paraelectric state was evidenced for unkown Rhombohedral *X* or Cubic *X* phase [8,12] of the phase diagram associated with two branches. The further study of the hysteresis loops across the transition temperature (about 340K) for PMN-PT (*x*=0.21) crystals were performed. The square shape of P-E loop was recorded at 35°C well below the transition temperature, which shows the existence of the ferroelectric phase at 300 K. Hysteresis loops became slim and then nonlinear at elevated temperatures with a phase transition at about 70°C. It was well considered during Rietveld refinement for the PMN end to PMN-PT (*x*=0.21) which supposed the phase evolution of a cubic to rhombohedral one. A detailed structure analysis carried out for these materials revealed the development of a ferroelectric state. For the whole series of ferroelectric to paraelectric phase, qualitative phase analysis using Rietveld method and electron diffraction are further performed for compositions in the two temperature regions which will be dedicated to the phase identification and structure stability of PMN-PT solid solution.

## Concluding remarks

The structure changes of PMN-PT solid solution have been investigated and the structure refinements were based on neutron powder diffraction data at 300 K and 3 K by the full pattern Rietveld analysis. The two powders of PMN and PMN-PT (*x*=0.21) prepared from crystals were not isostructural, but exist in the space groups *Pm3m* and *R3mH*, respectively. Both hysteresis loops and domain contrast from electron diffraction show the reliability of the presented structural models. A comparison between these two series shed light on the structural development with different symmetries, even though a close resemblance exists in the phase diagram.

# References


1. Smolensky, G.A., 1981, *Ferroelectrics and Related Materials* (New York: Gordon and Breach).
2. Service, R.F., 1997, *Science*, **275**, 1878.
3. Blinc, R., Laguta, V.V. & Zalar B., 2003, *Phys. Rev. Lett*., **91**, 247601.
4. Blinc, R., Laguta, V.V., Zalar, B. & Banys J., 2006, *J. Mater. Sci*., **41**, 27.
5. Jeong, I.K., Darling, T.W., Lee, J.K., Proffen, T., Heffner, R.H., Park, J.S., Hong, K.S., Dmowski,W. & Egami, T., 2005, *Phys. Rev. Lett*., **94**, 147602.
6. Hirota, K., Ye, Z.-G., Wakimoto, S., Gehring, P.M. & Shirane, G., 2002, *Phys. Rev.*
7. *B*, **65**, 104105.
8. Conlon, K.H., Luo, H., Viehland, D., Li, J.F., Whan, T., Fox, J.H., Stock, C. & Shirane, G., 2004, *Phys. Rev. B*, **70**, 172204.
9. Wang, H., Pan, X., Lin, D., Luo, H., Yin, Z. & Elouadi, B., 2007, *Appl. Phys. Lett*., **90**, 252902.
10. Tu, C.-S.,Chien, R.R.,Wang, F., Schmidt, V.H. & Han, P.,2004, *Phys. Rev. B*, **70**, 220103.
11. Wang H., Zhu J., Lu N., Bokov A. A., Ye Z. G., and Zhang X. W., 2006, *Appl. Phys. Lett.* **89**, 042908.
12. Noheda, B. & Cox, D.E., 2006, *Phase Transit*., **79**, 5.
13. Xu, G.,Viehland, D., Li, J.F., Gehring, P. & Shirane, G., 2003, *Phys. Rev. B*, **68**, 212410.
14. Xu G., Hiraka H., Shirane G. & Ohwada, K., 2004, *Appl. Phys. Lett*., **84**, 3975.
15. Singh, A.K., Pandey, D. & Zaharko, O., 2006, *Phys. Rev. B*, ***74***, 024101.
16. Luo, H., Shen, G., Wang, P., Le, X. & Yin, Z., 1997, *J. Inorg. Mater.*, **12**, 768.
17. Hölzel M., Senyshyn A., Gilles R.,Boysen H., Fuess H.,2007, *Neutron News* **18**, 23.
18. Roisnel, T. & Rodríquez-Carvajal, J., 2001, *Mater. Sci. Forum*, **378-381**, 118.
19. Schmitt, L.A., Schönau, K.A., Theissmann, R., Fuess, H., Kungl, H., & Hoffmann, M.J., 2007, *J. Appl. Phys.*, **101**, 074107.
20. De Mathan, N., Husson, E., Calvarin, G., Gavarri, J.R., Hewat, A.W. & Morell, A., 1991, *J. Phys. Condens. Matter*. , **3**, 8159.
21. Miao, S., Zhu, J., Zhang, X. & Cheng, Z.-Y., 2002, *Phys. Rev. B*, **65**, 052101.


**Acknowledgements.** This work is supported by the European project "Network of excellence" program "FAME: Functionalised Advanced Materials Engineering of Hybrids and Ceramics" and Deutsche Forschungsgemeinschaft SFB 595 "Electrical fatigue of functional materials". The neutron powder diffractometer SPODI is operated in the frame of the ''Instrumentation at large-scale facilities for condensed matter research'' program of the Bundesministerium fuer Bildung und Forschung under grant No. 03FU7DAR.